# Flow stagnation at Enceladus: The effects of neutral gas and charged dust

N. Omidi,[1] R. L. Tokar,[2] T. Averkamp,[3] D. A. Gurnett,[3] W. S. Kurth,[3] and Z. Wang[3]

Received 29 December 2011; revised 3 April 2012; accepted 16 May 2012; published 29 June 2012.

[1] Enceladus is one of Saturn's most active moons. It ejects neutral gas and dust particles from its southern plumes with velocities of hundreds of meters per second. The interaction between the ejected material and the corotating plasma in Saturn's magnetosphere leads to flow deceleration in ways that remain to be understood. The most effective mechanism for the interaction between the corotating plasma and the neutral gas is charge exchange which replaces the hotter corotating ions with nearly stationary cold ions that are subsequently accelerated by the motional electric field. Dust particles in the plume can become electrically charged through electron absorption and couple to the plasma through the motional electric field. The objective of this study is to determine the level of flow deceleration associated with each of these processes using Cassini RPWS dust impact rates, Cassini Plasma Spectrometer (CAPS) plasma data, and 3-D electromagnetic hybrid (kinetic ions, fluid electrons) simulations. Hybrid simulations show that the degree of flow deceleration by charged dust varies considerably with the spatial distribution of dust particles. Based on the RPWS observations of dust impacts during the E7 Cassini flyby of Enceladus, we have constructed a dust model consisting of multiple plumes. Using this model in the hybrid simulation shows that when the dust density is high enough for complete absorption of electrons at the point of maximum dust density, the corotating flow is decelerated by only a few km/s. This is not sufficient to account for the CAPS observation of flow stagnation in the interaction region. On the other hand, charge exchange with neutral gas plumes similar to the modeled dust plumes but with base (plume opening) densities of $\sim 10^9$ cm$^{-3}$ result in flow deceleration similar to that observed by CAPS. The results indicate that charge exchange with neutral gas is the dominant mechanism for flow deceleration at Enceladus.

**Citation:** Omidi, N., R. L. Tokar, T. Averkamp, D. A. Gurnett, W. S. Kurth, and Z. Wang (2012), Flow stagnation at Enceladus: The effects of neutral gas and charged dust, *J. Geophys. Res.*, *117*, A06230, doi:10.1029/2011JA017488.

## 1. Introduction

[2] Observations by the Cassini spacecraft have demonstrated that Saturn's moon Enceladus is highly active. It ejects one or more plumes of gas and dust from surface fractures in the southern polar region [*Porco et al.*, 2006; *Spencer et al.*, 2006; *Waite et al.*, 2006; *Hansen et al.*, 2006]. Charge exchange between the corotating plasma and neutral gas creates freshly produced ions which causes changes in the bulk plasma flow and magnetic field properties [*Dougherty et al.*, 2006; *Tokar et al.*, 2006]. The neutral gas plumes are a major contributor to Saturn's magnetospheric plasma and dynamics [e.g., *Kivelson*, 2006; *Jones et al.*, 2006; *Pontius and Hill*, 2006]. The plume neutrals are ejected at speeds of a few hundred m/s [see e.g., *Burger et al.*, 2007; *Smith et al.*, 2010] which is much smaller than the orbital velocity of Enceladus ~12.6 km/s. In contrast, the plasma corotation speed is ~39 km/s at the orbit of Enceladus. The corotating plasma consists primarily of water group ions ($O^+$, $OH^+$, $H2O^+$, $H3O^+$), light ions ($H^+$, $H2^+$) and electrons. Charge exchange between the plume water vapor and the plasma is the dominant means of interaction, although ion neutral chemistry is also present [*Tokar et al.*, 2006, 2009; *Cravens et al.*, 2009]. Given that the neutral gas and the corotating plasma are primarily water group, the process of charge exchange does not modify the plasma mass density in any appreciable way. However, due to the lower velocity of the newly created ions and the escape of the newly created neutrals from the system, charge exchange is associated with a reduction in plasma momentum and energy.

[3] A number of investigations have been carried out in the past to determine the amount of neutral gas in the southern plume(s) and the associated number of freshly created ions due to charge exchange. *Khurana et al.* [2007]

[1]Solana Scientific Inc., Solana Beach, California, USA.
[2]Los Alamos National Laboratory, Los Alamos, New Mexico, USA.
[3]Department of Physics and Astronomy, University of Iowa, Iowa City, Iowa, USA.

Corresponding author: N. Omidi, Solana Scientific Inc., 777 Pacific Coast Hwy., Solana Beach, CA 92075, USA. (omidi@solanasci.com)


0148-0227/12/2011JA017488

used the magnetic field perturbations observed in the first three flybys of Enceladus to determine the magnitude of the associated currents and thereby deduced the amount of plasma mass loading and the implications for the neutrals in the plume(s). They concluded that the mass picked up by the plasma within 5 $R_E$ (Enceladus Radii) of Enceladus is less than 3 kg/s. The model of *Pontius and Hill* [2006] used the observed flow deflections during the Enceladus E2 (14 July 2005) encounter to arrive at a total mass loading rate of more than 100 kg/s of new water molecules ($>4 \times 10^{27}$ $H_2O$/s). *Saur et al.* [2008] used the two-fluid, asymmetric model developed by *Saur et al.* [2007] and Enceladus flyby data to estimate the neutral gas content of the plumes. They arrived at total plume contents (plume density integrated over the plume volume) of $\sim 7 \times 10^{32}$ during E0 and $9 \times 10^{31}$ water molecules during the E1 and E2 flybys which corresponded to the creation of $\sim$3 and 0.2 kg/s of new born ions, respectively.

[4] In previous work directly related to the present study, *Omidi et al.* [2010a] used 3-D electromagnetic hybrid (kinetic ions, fluid electrons) simulations to investigate the nature of the interaction between the corotating plasma and the body of the moon, the extended neutral cloud and the plume of neutral gas in the southern hemisphere. The results showed that plasma absorption by the moon resulted in a downstream density cavity and a rarefaction wave. The presence of the extended neutral cloud resulted in the generation of ion cyclotron waves [e.g., *Leisner et al.*, 2006; *Cowee et al.*, 2009] and uniform deceleration of the plasma by a few km/s. The neutral gas in the plume modified the interaction region when its density corresponded to the production of $\sim$0.08 kg/s of newborn ions. When this value increased to 0.8 kg/s or more an Alfvén wave [*Neubauer*, 1980] (typically referred to as Alfvén wing) was also generated. Comparing the simulation results to Cassini Plasma Spectrometer (CAPS) observations by *Tokar et al.*, [2009] showed that plumes corresponding to the creation of $\sim$4 kg/s or more of new born ions were necessary to account for the observed flow speed of a maximum of a few km/s within the plume. *Kriegel et al.* [2009] used 3-D hybrid simulations to investigate the Enceladus interaction region during the Cassini E1 and E2 encounters and through comparisons with the magnetic field data concluded there was a neutral gas plume oriented toward downstream and away from Saturn.

[5] *Jia et al.* [2010a] examined the Cassini magnetometer data during the Enceladus encounters during 2008 and found changes in the field signatures due to time variability of the neutral gas in the plume. In a following study, *Jia et al.* [2010b] modeled the interaction between the plasma disk and Enceladus with its neutral plume using 3-D MHD simulations. By comparing the results with the magnetometer observations during two Cassini flybys, one in 2005 and one in 2008, a collection of parametric studies were presented. These comparisons illustrated the effects of the gas production rate, chemical reaction rates (predominantly charge exchange), upstream conditions and shape of the plume on the field perturbation. These results were extended in *Jia et al.* [2010c] who compared the MHD simulation results to the magnetic field measurements during the seven Enceladus flybys from 2005 to 2008. Based on this comparison they concluded that electron impact ionization rates and charge-exchange rates must decrease significantly close to the origin of the plume. Accordingly, such a decrease explained why the pickup process was less efficient in the plume region. Also, the magnetometer observations suggested that the center of momentum loading was about 2 $R_E$ below the south pole. They also suggested a need for the development of a multispecies model as well as a global magnetosphere code in order to accurately and self-consistently calculate all the relevant dynamic processes.

[6] Due to the collisionless nature of the corotating plasma, in order for a dust particle to interact with the plasma it is necessary for it to become electrically charged. Upon becoming charged, the dust particle couples to the plasma through the motional electric field and is accelerated to velocities of the order of the corotation speed on time scales of its cyclotron period. This in turn results in the deceleration of the plasma. Based on Cassini observations, two distinct methods of dust charging have been suggested. *Farrell et al.* [2009] examined the Radio Plasma Wave System (RPWS) measurements of the upper hybrid waves and noted a down shift in their frequency during the E3 Enceladus flyby. Since the upper hybrid frequency follows the electron density it was suggested that electron absorption by dust was responsible for the observed down shift in the upper hybrid frequency. This implied negative charging of the dust particles. *Shafiq et al.* [2011] examined the Langmuir probe data during the E3 encounter and reported ion densities increasing from the background level of $10^2$ $cm^{-3}$ to $10^5$ $cm^{-3}$ just before the closest approach. On the other hand electron densities in the same region were found to be two orders of magnitude smaller. It was assumed by *Shafiq et al.* [2011] that this difference was due to electron absorption by dust particles. The presence of charged dust in the vicinity of Enceladus has also been reported by *Jones et al.* [2009] who suggested that both positive and negatively charged dust particles were produced within the plume due to collisions and triboelectric charging. Based on the analysis of CAPS data, *Hill et al.* [2012] suggested the presence of nanometer-sized dust particles with negative charge density of up to $\sim$2600 e/$cm^3$ during the E3 encounter.

[7] *Omidi et al.* [2010b] used 3-D hybrid simulations of a spherically symmetric dust cloud with a radially decreasing density to determine how the size of the interaction region varied with the level of electron absorption. The flow velocities obtained from simulations with various levels of electron absorption were compared to the CAPS data during E3 flyby. It was shown that for maximum electron absorption (occurring above the surface of Enceladus) of more than 20%, the size of the interaction region was too large compared to the CAPS observations. *Simon et al.* [2011] and *Kriegel et al.* [2011] used analytic theory and hybrid simulations respectively to examine the impacts of negatively charged dust on the magnetic structure of the Alfvén wing. They suggested that the presence of large levels of negatively charged dust particles resulted in a negative Hall conductivity and the modification of the magnetic perturbations associated with the Alfvén wing.

[8] The purpose of this investigation is to extend the results of *Omidi et al.* [2010b] by constraining the shape and orientation of the dust and neutral gas plumes and constructing models using dust impact rates detected by Cassini RPWS instrument. Using these plume models in 3-D hybrid simulations with different levels of charged dust and neutral

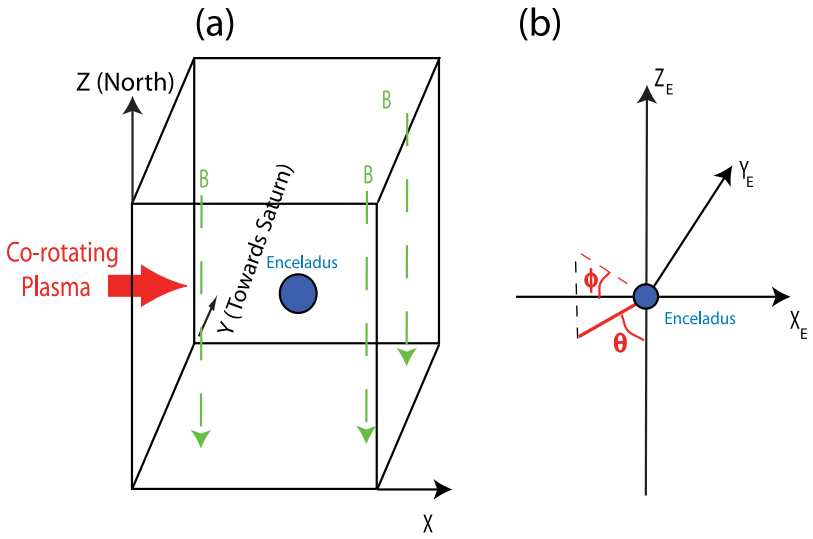


**Figure 1.** (a) The hybrid simulation model and the coordinate system with X along the corotation flow, Y toward Saturn, and Z along north. (b) The Enceladus centered coordinate system used for dust and neutral gas plumes. The angle $\theta$ is measured with respect to the $-Z_E$ axis, and $\varphi$ is measured relative to $-X_E$ axis.

gas density their effects on the flow properties of the corotating plasma is examined and compared to CAPS data. Through this comparison we establish the role of charged dust and neutral gas in flow deceleration during the Cassini E7 encounter.

## 2. Model Description

### 2.1. Hybrid Simulation Model

[9] The electromagnetic hybrid (kinetic ions, fluid electrons) code used in this study is the same as that used in *Omidi et al.* [2010a, 2010b] and is described in considerable detail in *Omidi et al.* [2010a]. Here, we provide a brief overview of the hybrid model in general and that used in this study.

[10] In hybrid simulations, ions are treated kinetically and may consist of one or more populations or species (e.g., differing temperature, mass, charge, etc.). Electrons are treated as a massless, charge neutralizing fluid. The four equations that are solved include Ampere's law without the displacement current (called the Darwin approximation) so that high-frequency light waves are eliminated and Faraday's law. The third equation is the electron momentum equation with electron mass equal to zero, which leads to the generalized Ohm's law that includes electron pressure gradients and a resistive term that represents ion-electron interactions. Here, the resistive length scale is ~0.005 ion skin depth, $c/\omega_p$, where c is the speed of light and $\omega_p$ is the ion plasma frequency ($c/\omega_p$ ~50 km at Enceladus). This resistive length scale is much smaller than the cell size which ensures that the results are not influenced by the choice of resistivity. The electron current is related to the ion current and magnetic field by Ampere's law. The electron pressure is determined assuming isothermal electrons. The fourth equation is the Lorenz force law that governs the motion of the ions. Standard Particle-in-Cell (PIC) methods are used to advance the ions. By virtue of the kinetic treatment of ions, hybrid simulations provide information on the nature of the interaction region on ion temporal and spatial scales and include low-frequency waves such as magnetosonic and Alfvén ion cyclotron waves.

[11] Figure 1a shows a schematic of the simulation box and the coordinate system used in the model with the *x* axis along the direction of the corotation velocity, the *y* axis pointing toward Saturn and Z along north and completing a right-handed coordinate system. The simulations are performed in the rest frame of Enceladus with corotating plasma injected from the left (X = 0) boundary with velocity of 0.1 $V_A$ (24–30 km/s). The boundary conditions used are described in *Omidi et al.* [2010a, 2010b]. Here we note that the boundary conditions on the top and bottom boundaries (Z = 0 and L_z, the size in Z direction) keep the corotation electric field constant which mimics the corotation of the magnetic field due to connection to the ionosphere. Saturn's (background) magnetic field is assumed to be uniform in the simulation domain at a value of 325 nT. The corotating plasma is assumed to consist of $O^+$ ions with plasma beta of 0.006. Given that this study is not concerned with ion chemistry, the use of single ion species ($O^+$) to represent the corotating plasma which contains water group ions is a satisfactory approximation and does not impact the conclusions reached here. The results presented here correspond to a maximum system size of X = 95, Y = 23 and Z = 190 $R_E$. To facilitate the comparisons between the hybrid simulations and the CAPS spectrogram data, we have performed high-resolution (cell size of 0.25 ion skin depth) simulations with hundreds of particles per cell that allow for the generation of simulated ion energy spectrograms.

[12] The body of Enceladus forms a plasma absorbing obstacle to the flow so that all ions hitting its surface are lost. The volume inside the moon lies outside of the simulation domain in that no currents exist in this region and the initial magnetic field is kept constant. This implies that all changes in the magnetic field outside Enceladus are associated with the currents generated in the plasma. When included in the run, Saturn's extended neutral cloud forms an obstacle

through charge exchange between the ions and neutrals. This process is reproduced in the simulations by changing the velocity of a fraction of ions randomly between zero and 500 m/s (representing the velocity of the neutral gas before ionization) every time step. We note that the results and conclusions reached in this study would not be affected with the choice of larger than 500 m/s velocities (e.g., 1 km/s) as long as the energy of the neutral gas is considerably smaller than that of the corotating ions that have energies of 100 s of eV. The fraction of ions going through this charge exchange process depends on the density of the neutrals and the cross section for ion-neutral charge exchange. We use a cross section of 36 Angstrom squared provided by *Burger et al.* [2007] for charge exchange between $O^+$ and $H_2O$ at a relative velocity of 26 km/s. We note that this is a simplifying assumption that does not include the variations of the cross section with the relative velocity between the ions and the neutral gas particles. The interaction between the corotating plasma and the neutral gas associated with the plumes in the southern polar region is also modeled as charge exchange. The model used for the spatial distribution of the neutral gas in the plume is described in section 2.3.

[13] Charged dust particles are treated as ions (PIC) with negative charge due to electron absorption. Because the ion skin depth is much larger than the Debye length (a few meters) in the hybrid model charge neutrality is enforced. As a result, when the dust particles are charged negatively as in this study the density of electrons is accordingly reduced. While in reality, the size, mass and level of charge for dust particles varies considerably [e.g., *Shafiq et al.*, 2011] in the hybrid model the dust particles are approximated as a cloud with size equal to the cell size and a specified charge to mass ratio. This treatment is similar to how plasma particles are treated in PIC simulations. In this study we assume a charge to mass ratio of −1/16,000 (e/atomic mass). This choice ensures that on the time scale of the simulations (300–400 $\Omega_{O+}^{-1}$ where $\Omega_{O+}$ is the angular cyclotron frequency of singly charged oxygen) the dust particles are nearly stationary and the use of heavier dust particles would not impact the conclusions reached in this study. The number of dust particles in each cell is determined by the spatial distribution of the dust particles in the model. The dust models used in this study are described in the next section.

### 2.2. Charged Dust Models

[14] Three models have been utilized for the spatial distribution of dust particles in the hybrid simulations. Two are theoretical models that demonstrate the importance of the spatial distribution of the dust particles on the size and location of the interaction region and the third is based on dust impact rates measured by the RPWS instrument aboard the Cassini spacecraft. In a spherically symmetric model, the dust number density $N_D$ is given by:

$$N_D = N_{Do}/R^2 \quad (1)$$

where $N_{Do}$ is the density at the surface of Enceladus and R is the radial distance normalized to $R_E$. We also utilize a cone model for the dust particles defined by:

$$N_D = N_{Do} \times S(\psi_o)/R^2 \quad (2)$$

where S is the Step function and is equal to 1 when $\psi < \psi_o$ and is zero otherwise. The angle $\psi$ is measured relative to the cone axis depicted as a solid red line in Figure 1b. The angle $\psi_o$ in equation (2) specifies the width of the cone so that when $\psi > \psi_o$ dust density is zero. The cone axis makes an angle $\theta$ with the negative $Z_E$ axis (Enceladus centered coordinate system shown in Figure 1b). The projection of this axis onto the $X_E$–$Y_E$ plane makes an angle $\varphi$ with the negative $X_E$ axis. The use of a Step function implies a uniform density within the cone for a given R and we therefore, refer to equation (2) as a uniform cone model.

[15] In the remainder of this section we describe the dust model constructed from the RPWS measurements. Figure 2 shows the RPWS wide band receiver spectrogram during the 2 November 2009 (E7) Cassini encounter with Enceladus. Indicated on the figure are the signals detected by RPWS due to dust impacts in the vicinity of Enceladus between ∼07:40 and 07:44 UT [*Kurth et al.*, 2006; *Wang et al.*, 2006]. Dust impact on spacecraft generates a unique signature in the electric field wave form data that allows one to measure the number of impacts per unit time [see e.g., Gurnett *et al.*, 1987]. This detection method can be used to estimate the density of ∼micron sized dust particles and their spatial distribution. Figures 3a and 3b show the RPWS dust impact rates at low and high levels of sensitivity between 07:40 and 07:44 UT respectively. The low- and high-sensitivity impact rates are related to the changes in the instrument gain and the resulting change in sensitivity to large versus small particles during the flyby. At the low sensitivity (low gain), relatively larger sized dust particles are detected as compared to the high sensitivity (high gain) when smaller size dust particles are detected. Inclusion of the impacts during "high sensitivity" show a lot more particles in the wings of the distribution function as illustrated in Figure 3. The orbital properties of the Cassini spacecraft relative to Enceladus are shown in the remaining panels in Figure 3. The angles $\theta$ and $\varphi$ are measured as illustrated in Figure 1b with the red solid line (in this case) representing the instantaneous radial vector.

[16] To model the dust impact rates in Figures 3a and 3b we have used multiple dust plumes each defined by the following equation.

$$N_D = N_{Do} \exp(-\psi/\psi_o)/R^n \quad (3)$$

In contrast to the uniform cone model described by equation (2), the cone in equation (3) is diffused in that for a given R, the density is maximum on the cone axis and decreases with $\psi$. Note that $\psi_o$ in equation (3) specifies the width of the cone, however, in contrast to equation (2) dust particles are present for $\psi > \psi_o$ in the diffused dust model. In addition, equation (3) allows for a variety of radial profiles for the dust particles through the choice of parameter 'n'. The use of multiple plumes is well justified by Cassini images of Enceladus' southern polar region [see e.g., *Lee et al.*, 2010, Figure 1].

[17] Starting with one plume, dust impact rates along the Cassini trajectory were obtained for a wide range of plume parameters $N_{Do}$, $\theta$, $\varphi$, $\psi_o$, and n and compared to the low- and high-sensitivity impact rates. Figures 4a and 4c show comparisons of the calculated (in red) and observed low- and high-sensitivity impact rates using one plume. Figure 4a

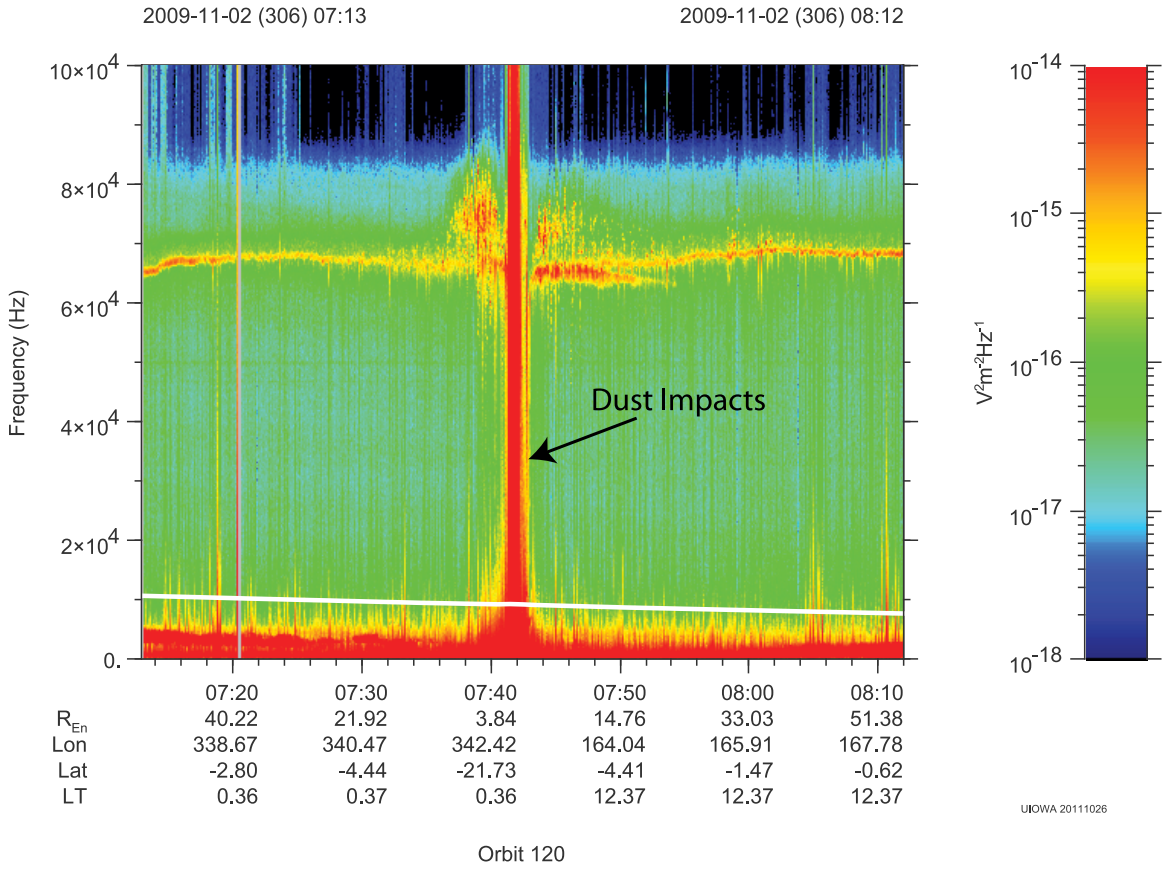


**Figure 2.** RPWS spectrogram during the E7 flyby of Enceladus showing the signals detected due to dust impacts with Cassini.

shows a relatively good comparison in terms of time interval when appreciable dust impacts are observed and also the maximum number of dust impacts. However, a better match to the low-sensitivity impact rates is obtained (Figure 4b) by using two dust plumes with parameters defined for plumes # 2 and 3 in Table 1 which better reproduce the shoulder present in the observed impact rates. Similarly, Figure 4c illustrates the difficulty in reproducing the observed high-sensitivity impact rates using a single plume. In order to obtain a calculated dust impact rate profile that reproduces the main features of the high-sensitivity impact rates it was necessary to use three dust plumes with parameters defined for plumes # 4, 5 and 6 in Table 1. A comparison between the observed and modeled high-sensitivity dust impact rates is shown in Figure 4d. In all cases, the parameter n in equation (3) is set to 2 implying $R^{-2}$ density profile. In general, we find that variations of plume parameters $\theta$, $\varphi$, $\psi_o$ by a few degrees ($\sim$2–5°) result in appreciable changes in the dust impact rates profile along the Cassini trajectory.

[18] The base densities $N_{Do}$ for the plume numbers 2 through 6 used in Figure 4 are related to the dust impact rates through the effective cross section of the Cassini spacecraft. Given that most of the spacecraft is covered by a low-yield thermal blanket, we estimate the effective cross section to be $\sim$0.5 $m^{-2}$. The resulting base densities are of the order of $10^{-6}$ $cm^{-3}$ which is considerably smaller than the corotating plasma density of about 100 $cm^{-3}$. Observation by *Farrell et al.* [2009] of the absorption of most of the electrons by dust particles would require the presence of dust particles not detected by RPWS (likely due to a smaller size). In hybrid simulations, we allow for the presence of such dust particles by considering dust densities that result in local absorption of all electrons in the corotating plasma. In effect, we use the RPWS impact rates to constrain the spatial distribution of dust but allow for densities much higher than those detected by RPWS. Since dust particles of different sizes are expected to be present in a given plume, it is reasonable to use the same model for their spatial distribution.

### 2.3. Model for the Neutral Gas Plume

[19] The neutral gas plumes used in the hybrid simulations were modeled using either the uniform cone defined by equation (2) or the diffused cone defined by equation (3). The use of the same cone models (but different base densities) for dust and neutral gas is a reasonable approach given that plumes contain neutral gas and dust particles. The gas plumes extend to 12 $R_E$ and we have varied their base densities to compare the results to Cassini plasma observations as discussed in the next section.

## 3. Simulation Results

[20] To demonstrate the importance of the spatial distribution of the dust particles on the Enceladus interaction region, we show and compare results from runs with spherically symmetric and uniform cone dust plumes.

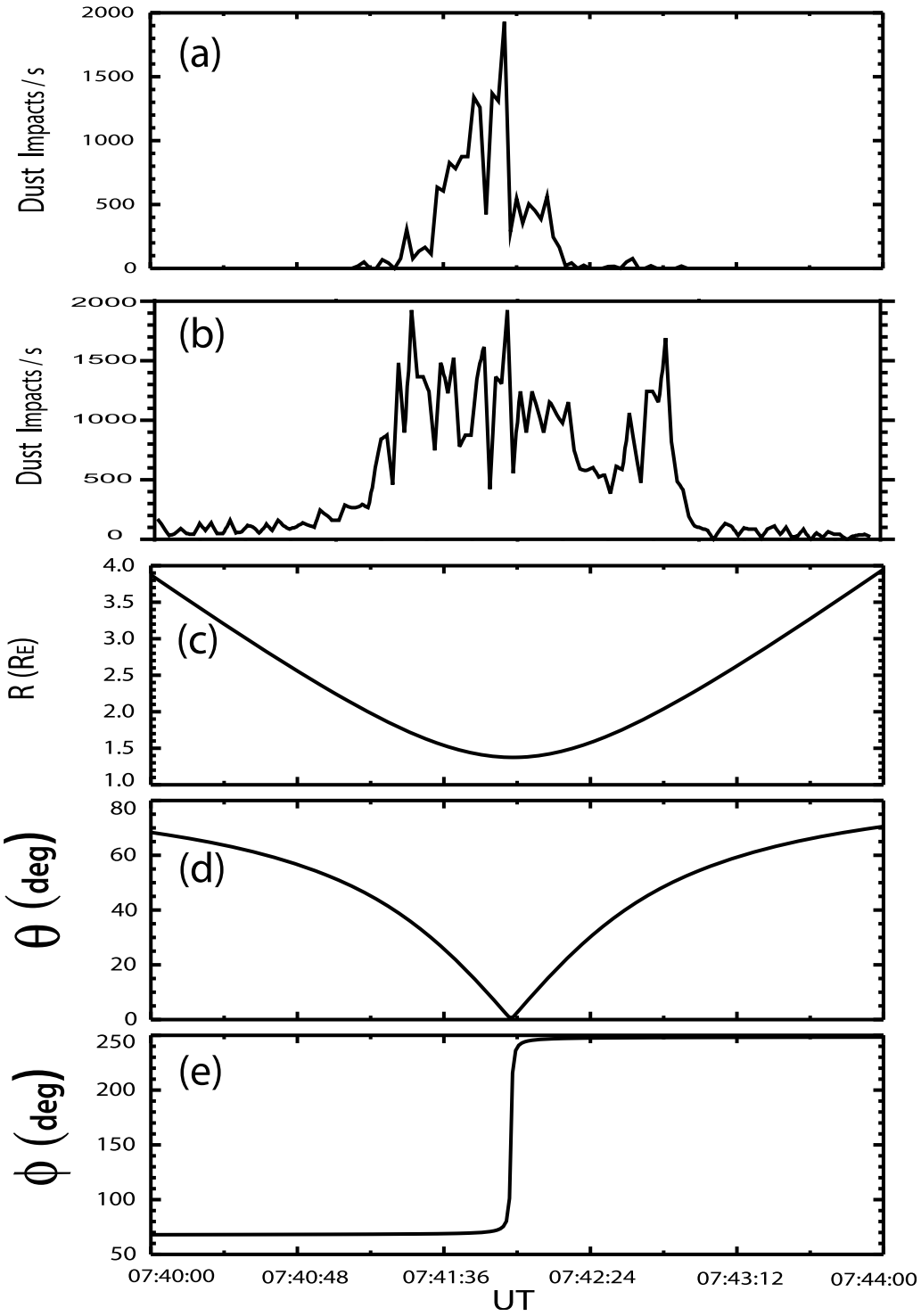


**Figure 3.** The (a) low- and (b) high-sensitivity RPWS impact rates during E7. (c–e) The radial distance of Cassini and the angles $\theta$ and $\varphi$ associated with the E7 trajectory.

Figure 5a shows the ion speed in the X direction in the X-Z plane at Y = 11.5 $R_E$ (containing Enceladus). The results are from a run with the neutral gas plume #1 in Table 2 and no charged dust. It is evident from Figure 5a that the flow velocity is reduced along the Alfvén wing and in a relatively narrow spatial region in the X direction. The lowest velocities are seen in the southern hemisphere within the gas plume. Figure 5b shows the results from a run with the same neutral gas plume as in Figure 5a and also a spherically symmetric dust cloud. This dust cloud has maximum charge density (above Enceladus' surface) corresponding to the absorption of

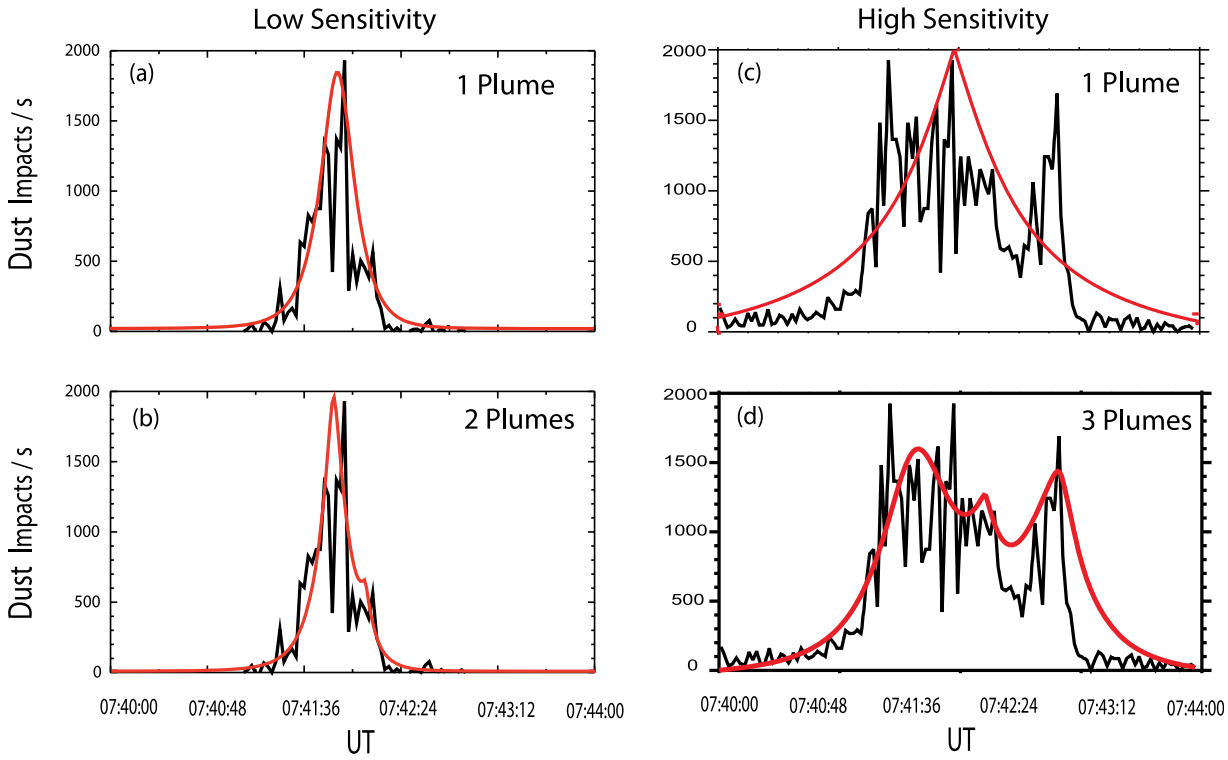


**Figure 4.** Comparisons of the measured (black line) and modeled (red line) dust impact rates for (a and b) low- and (c and d) high-sensitivity impact rates using one or more plumes.

50% of the electrons in the plasma. It is evident from Figure 5b that the presence of the charged dust has made the interaction region much wider in the X direction. In addition, the flow velocity is much lower and the plasma is nearly stagnant within the plume region.

[21] Figure 6a is the same as Figure 5a and shows the flow velocity in a run with no dust and the neutral gas plume #1 in Table 2. Figure 6b shows the flow velocity from a run with the same neutral gas model and also dust plume #1 in Table 1 containing as many dust particles as that in the spherical model in Figure 5b. It is evident from Figure 6 that the addition of charged dust lowers the flow velocity in the vicinity of the plume however, the size of the interaction region along the X direction is not increased in any appreciable way. This is in contrast to when the spherically symmetric dust model is used and demonstrates the significance of the spatial distribution of the dust in determining the characteristics of the interaction region. The results in Figure 6 show that when the neutral gas and charged dust have the same (or similar) spatial distribution they have a similar effect on flow deceleration. Examination of the electromagnetic signatures associated with the Alfvén wings in the two runs in Figure 6 also show similar characteristics associated with neutral gas and charged dust. As an example, Figure 7 shows the X component of the magnetic field from the two runs in Figure 6. Figures 7a and 7b correspond to the run with neutral gas only while Figures 7c and 7d include charged dust. It is evident that the overall structure of the Alfvén wing is similar in both runs although the addition of charged dust increases the maximum value of $B_X$ within the plume.

[22] The low- and high-sensitivity dust models derived from the RPWS measurements provide information on the spatial distribution of dust around Enceladus that we use in hybrid simulations to determine the associated level of flow deceleration. The largest level of flow deceleration occurs when the dust density is high enough for all the electrons in the corotating plasma to be absorbed locally. Accordingly, here we show results from runs with maximum dust density high enough to absorb all the electrons. In order to compare the results to observations we use the CAPS ion spectrogram data obtained during Cassini encounter with Enceladus on 2 November 2009 (E7). Figure 8a shows the RPWS low-sensitivity dust impact rates. Figures 8b–8d show the results from a hybrid run with the dust plumes #2 and #3 in Table 1 used to model the low-sensitivity impact rates. No neutral gas is included in this run. The figures show the fraction of negative charge on dust particles, the X component of the flow velocity and simulated ion energy spectrogram respectively. Figure 8e shows the CAPS ion spectrogram

**Table 1.** The Polar Angle $\theta$, Azimuthal Angle $\varphi$ (Illustrated in Figure 1b), Angle $\psi$, and Type of Cone for the Six Dust Plumes Used in the Study

| Plume | $\theta$ | $\varphi$ | $\psi$ | Cone Type |
|---|---|---|---|---|
| 1 | 0 | 0 | 5° | Uniform |
| 2 | 10° | 60° | 10° | Diffused |
| 3 | 10° | 25° | 5° | Diffused |
| 4 | 30° | 40° | 20° | Diffused |
| 5 | 20° | 250° | 20° | Diffused |
| 6 | 51° | 250° | 10° | Diffused |

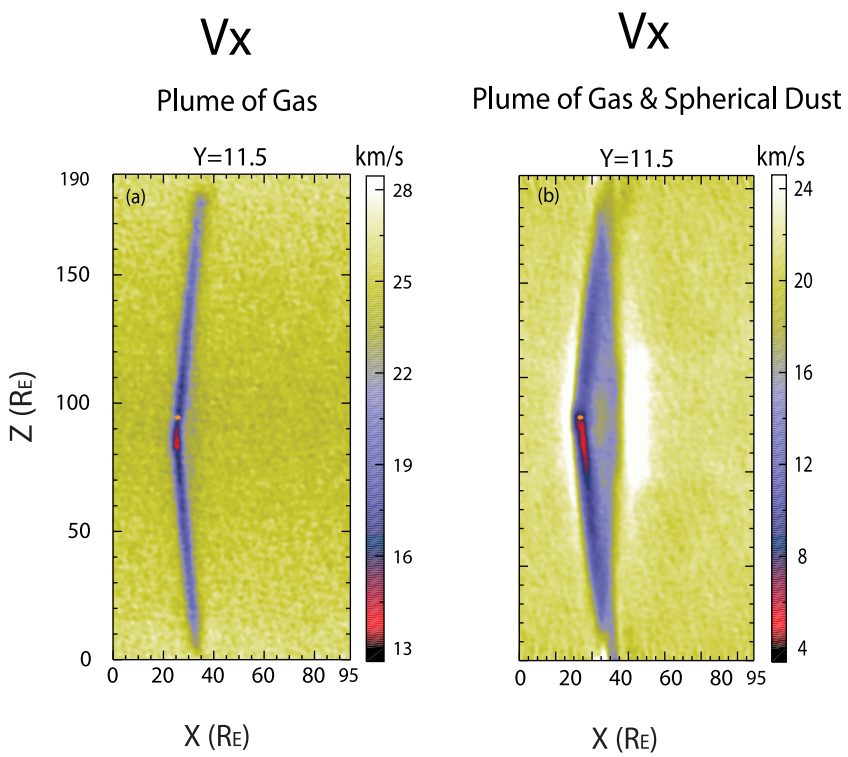


**Figure 5.** Ion velocity in the X direction from two hybrid simulation runs: (a) one having a neutral gas plume and (b) the other with both neutral gas and charged dust with a spherically symmetric spatial distribution.

data during the E7 encounter. The main interaction region is between ~07:41:30 and 07:43 where the plasma is nearly stagnant similar to that observed during the Enceladus E3 and E5 encounters [*Tokar et al.*, 2009]. It is evident that the RPWS dust impact rates and the fraction of negative charge on dust particles have a similar profile and at the time of the maximum impact rates ~40% of the negative charge in the corotating plasma is on the dust particles. Figure 8c shows the flow deceleration by a few km/s in the region of charged dust, however, this deceleration is too small to be noticeable in the simulated ion energy spectrogram as seen in Figure 8d. This is because the ion thermal velocity (~20 km/s) is comparable to the flow speed and a reduction of a few km/s in the flow speed represents a small change in ion energy.

[23] Figure 9 is in the same format as in Figure 8 except that it corresponds to a hybrid run with the RPWS high-sensitivity impact rates modeled by plumes #4, 5 and 6 in Table 1. The base densities used in this run are such that at the point of maximum dust density all electrons in the corotating plasma are absorbed. It is evident that compared to Figure 8 the size of the interaction region is larger in Figure 9, however, the levels of flow deceleration remain low at a few km/s and not sufficient to have an appreciable signature in the ion energy spectrogram. Figures 8 and 9 illustrate that using the RPWS constraints on the spatial distribution of charged dust and dust densities even orders of magnitude larger than those measured by RPWS does not lead to the level of flow deceleration observed by CAPS. To further substantiate this conclusion we have performed runs similar to those in Figures 8 and 9 but with dust plumes whose radial fall off is slower than $R^{-2}$. In these runs, dust particles were loaded with uniform probability in R. As a result, because of the increase in the size of the volume element within $\Delta R$ with R a density profile with much slower drop off as compared to $R^{-2}$ is obtained. The results of these runs are similar to those in Figures 8 and 9 and further indicate that charging of dust through electron absorption is not enough to account for the CAPS observations of flow deceleration during E7.

[24] Expecting that neutral gas and dust are ejected from the same plumes, we have used neutral gas plumes similar to the dust plumes #2–6 in Table 1 in the hybrid simulations. Using base densities of $10^6$ $cm^{-3}$ and larger, the impacts of these neutral gas plumes on the corotating plasma were investigated and compared to the CAPS plasma measurements. In particular, the level of flow deceleration and the time interval along the Cassini trajectory where flow deceleration occurs in the simulations were compared to the CAPS observations. The best agreement in terms of level and time interval of flow deceleration is obtained when plumes #2 and 3 in Table 2 are used with base densities of

**Table 2.** The Polar Angle $\theta$, Azimuthal Angle $\varphi$ (Illustrated in Figure 1b), Angle $\psi$, and Type of Cone for the Three Neutral Gas Plumes Used in the Study

| Plume | $\theta$ | $\varphi$ | $\psi$ | Cone Type |
|---|---|---|---|---|
| 1 | 0 | 0 | 5° | Uniform |
| 2 | 20° | 250° | 20° | Diffused |
| 3 | 51° | 250° | 10° | Diffused |

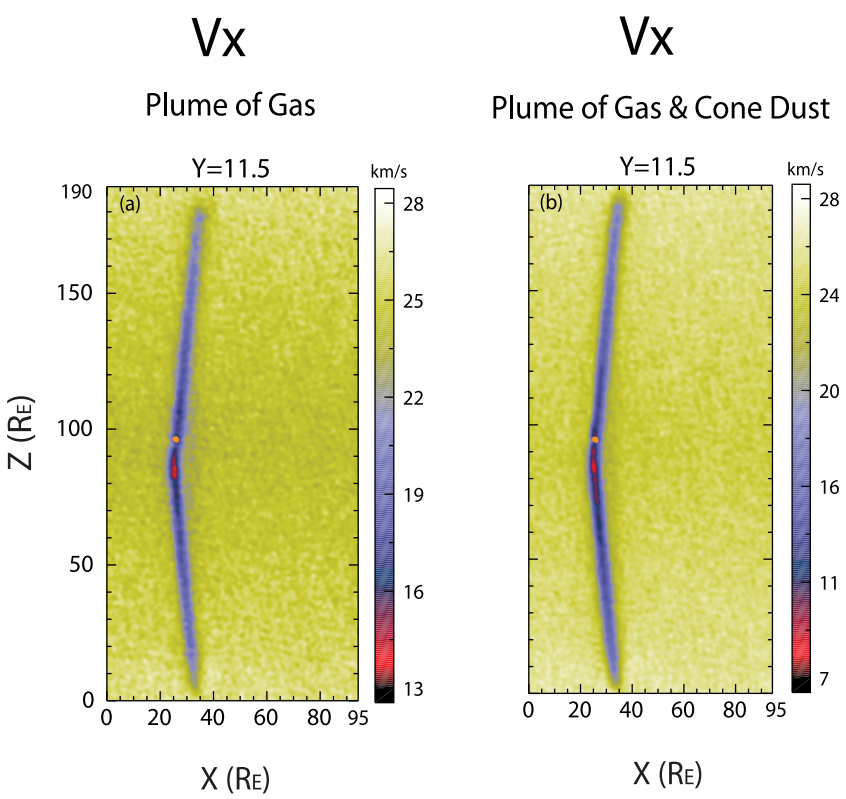


**Figure 6.** Ion velocity in the X direction from two hybrid simulation runs: (a) one having a neutral gas plume and (b) the other with both neutral gas and charged dust with a uniform cone model.

$1.6 \times 10^9$ and $2.4 \times 10^9$ cm$^{-3}$ respectively. Note that these plumes are similar to the dust plumes #5 and 6 in Table 1. The results of this run are shown in Figure 10a, which shows the corotating plasma density assuming a background level of 100 cm$^{-3}$. The flow velocity, shown in Figure 10b is reduced to a few km/s within the interaction region in anticorrelation with density which is enhanced within the interaction region. The simulated spectrogram in Figure 10c shows a drop in plasma energy due to charge exchange similar to that observed by the CAPS. Figure 10c also shows the presence of two regions of plasma deceleration and cooling that line up well with the two density peaks in Figure 10a. This occurs as a result of the presence of two neutral gas plumes in the simulation. A similar feature is also found in the CAPS spectrogram suggesting that it is due to the presence of two neutral gas plumes. It is evident that the use of the neutral gas plumes #2 and 3 in Table 2 lead to plasma signatures that agree well with the CAPS data in terms of the location and the duration of the interaction region, as well as level of flow deceleration and cooling.

## 4. Summary and Conclusions

[25] In this study, we have used Cassini RPWS and CAPS observations along with electromagnetic hybrid simulations to investigate the role of charge exchange with neutral gas, and electron absorption by dust particles on the observed stagnation of plasma flow near Enceladus. The process of charge exchange between the corotating plasma and neutral gas in the plume replaces the hotter moving ions with colder and nearly stationary (in the Enceladus rest frame) ions and as a result the flow velocity and temperature are reduced within the plume. Electron absorption by dust particles couples the charged dust to the corotating plasma through the motional electric field and results in flow deceleration. In both cases, local deceleration of the plasma and magnetic field launches a signal along the magnetic field to higher latitudes forming the Alfvén wing. Due to the low value of the plasma beta, flow deceleration occurs along the Alfvén wing extending the interaction region to large distances away from the southern plume(s). The size and structure of the Alfvén wing are heavily influenced by the spatial distribution of the neutral gas and charged dust. Here, we have used Cassini data to constrain the shape, orientation, and density of the dust and the neutral gas plumes and hybrid simulations to investigate their impacts on the deceleration of the corotating plasma.

[26] Hybrid simulations using a spherically symmetric model for the dust particles show the formation of a broad interaction region which does not agree with CAPS observations. Simulations also show that a uniform cone model with the same number of dust particles as in a spherical model results in a narrower interaction region. These results demonstrate the importance of the spatial distribution of charged dust and the need for models based on observations. Accordingly, the signals due to dust impacts detected by the RPWS were used to generate dust impact rates during the E7 encounter. Both the low- and high-sensitivity impact rates were used to model the spatial distribution of dust particles using two or three diffused cone plumes respectively. The base densities of these plumes are $\sim 10^{-6}$ cm$^{-3}$ which is about eight orders of magnitude smaller than the corotating

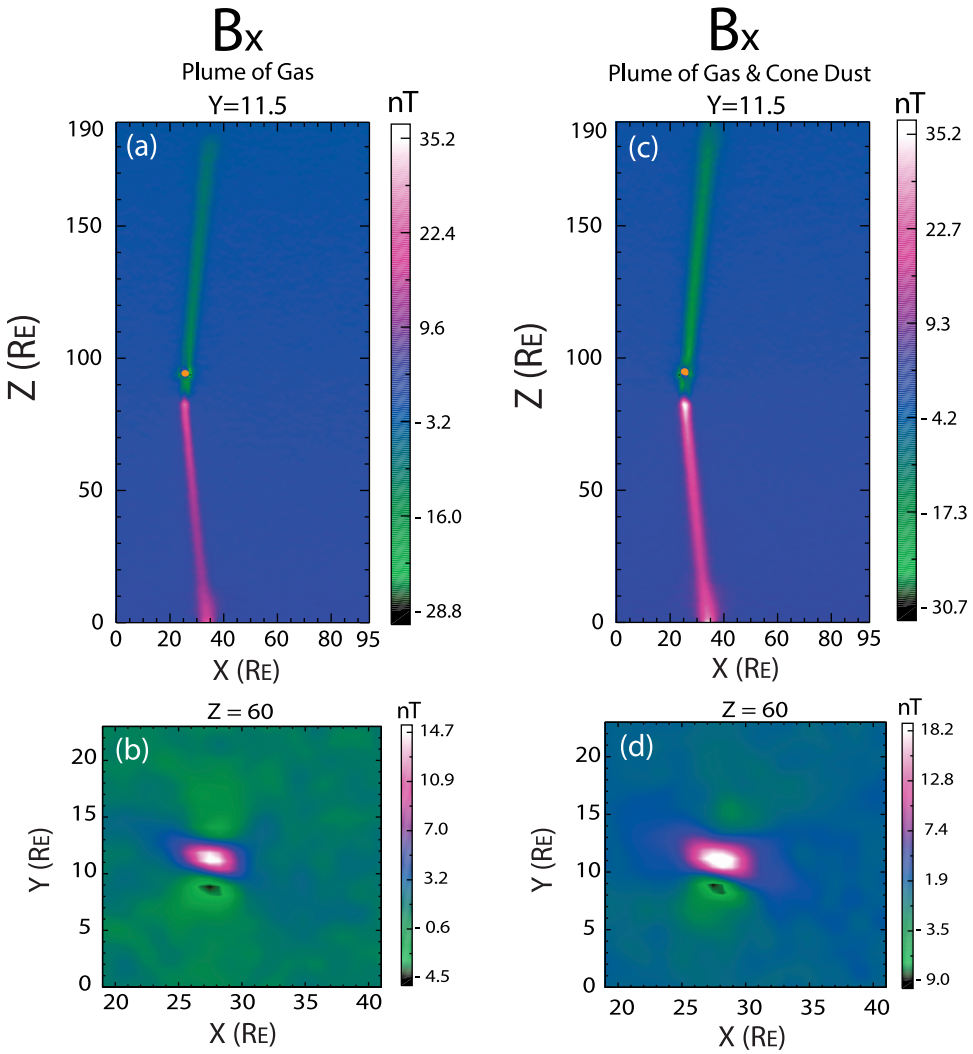


**Figure 7.** The X component of the magnetic field from the two runs in Figure 6. It is evident that the structure of the Alfvén wing remains similar in the absence and presence of charged dust.

plasma density. At such low levels, charging of the dust would have no impact on the plasma. Since, RPWS is sensitive to the detection of micron-sized dust particles we have used much larger base densities to allow for the presence of smaller sized dust particles not detected by the RPWS.

[27] Performing hybrid simulations with the low- and high-sensitivity RPWS dust models shows that when base densities of the plumes are high enough for the total absorption of the electrons at points of maximum dust density, flow is decelerated by a few km/s. This low level of deceleration is not sufficient to generate any detectable signatures in the simulated ion energy spectrogram and cannot account for the CAPS observations during the E7 encounter. To further substantiate this conclusion we performed hybrid simulations with the RPWS dust models modified to have a slower drop in density with radial distance as compared to $R^{-2}$. The results show no significant differences and the levels of flow deceleration remain low at a few km/s.

[28] Using neutral gas plumes similar to those modeled based on the RPWS dust impact rates we performed hybrid simulations with varying base densities and compared the results to the CAPS observations. When using the plumes #2 and 3 in Table 2 with base densities of $1.6 \times 10^9$ and $2.4 \times 10^9$ $cm^{-3}$ respectively we find the flow becomes nearly stagnant with corresponding increase in the corotating plasma density. The size and location of the interaction region agree well with the CAPS observations. Similarly, the simulated ion energy spectrogram has signatures similar to those observed by CAPS and provides support for the notion that two neutral gas plumes were responsible for the observed flow deceleration during the E7 encounter. We note that in modeling the high-sensitivity RPWS dust impact rates we used three active plumes (#4–6 in Table 1) two of which (#5 and 6) are similar to the neutral gas plumes responsible for the observed flow deceleration. We expect that dust plume #4 also contained neutral gas but not at densities high enough to impact the flow of the corotating plasma. According to our simulations, if plume #4 had a base density comparable to those of plumes #5 and 6 the time interval of the flow deceleration would have been longer than that observed by CAPS. Large variations in neutral gas plume densities associated with different source regions (Alexandria, Cairo and Damascus) have been reported by *Lee et al.* [2010] during the E3 encounter.

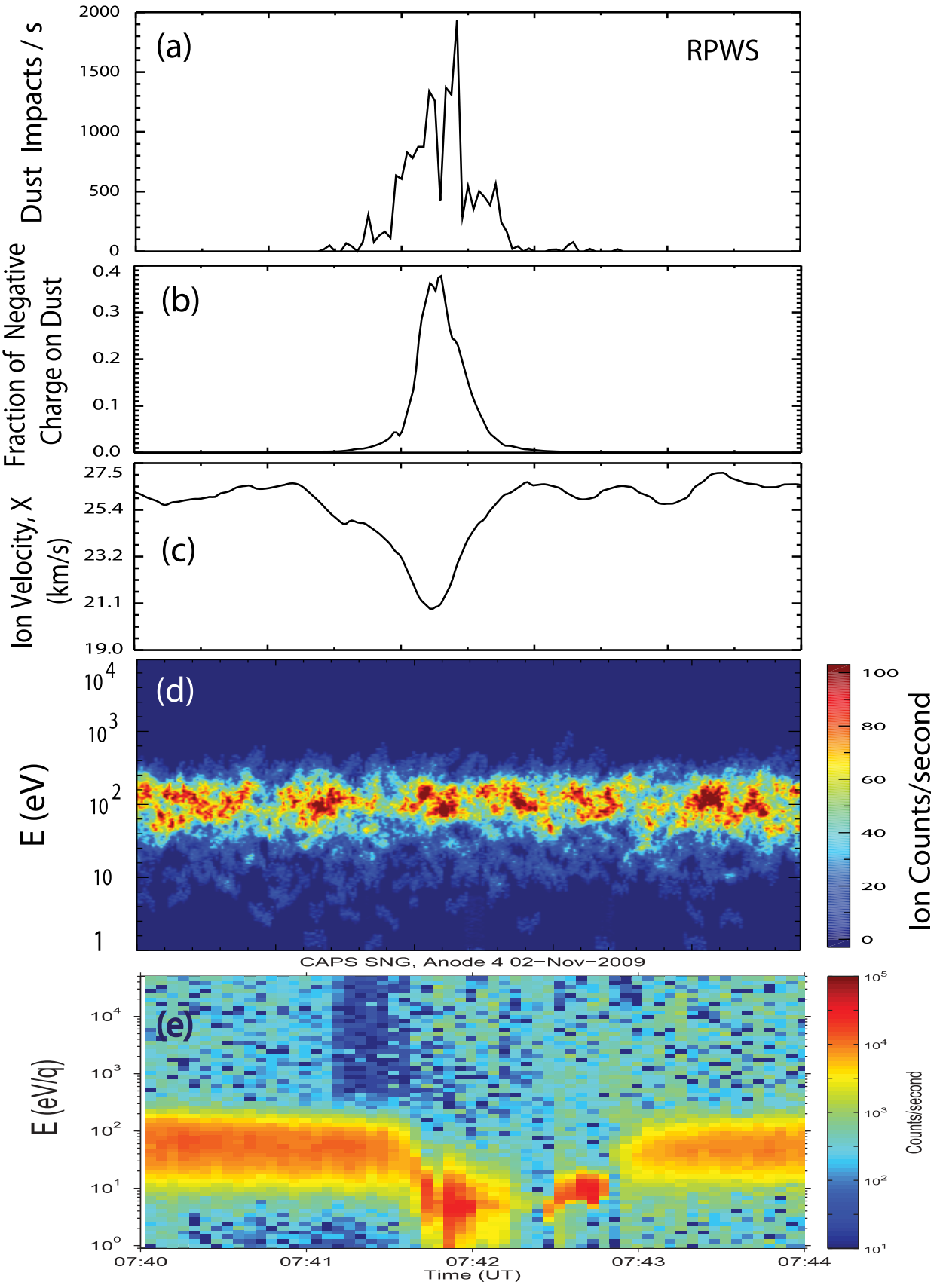


**Figure 8.** (a) RPWS low-sensitivity dust impact rates, (b) fraction of negative charge on dust, (c) X component of flow velocity, (d) simulated ion energy spectrogram, and (e) the CAPS ion energy spectrogram are shown.

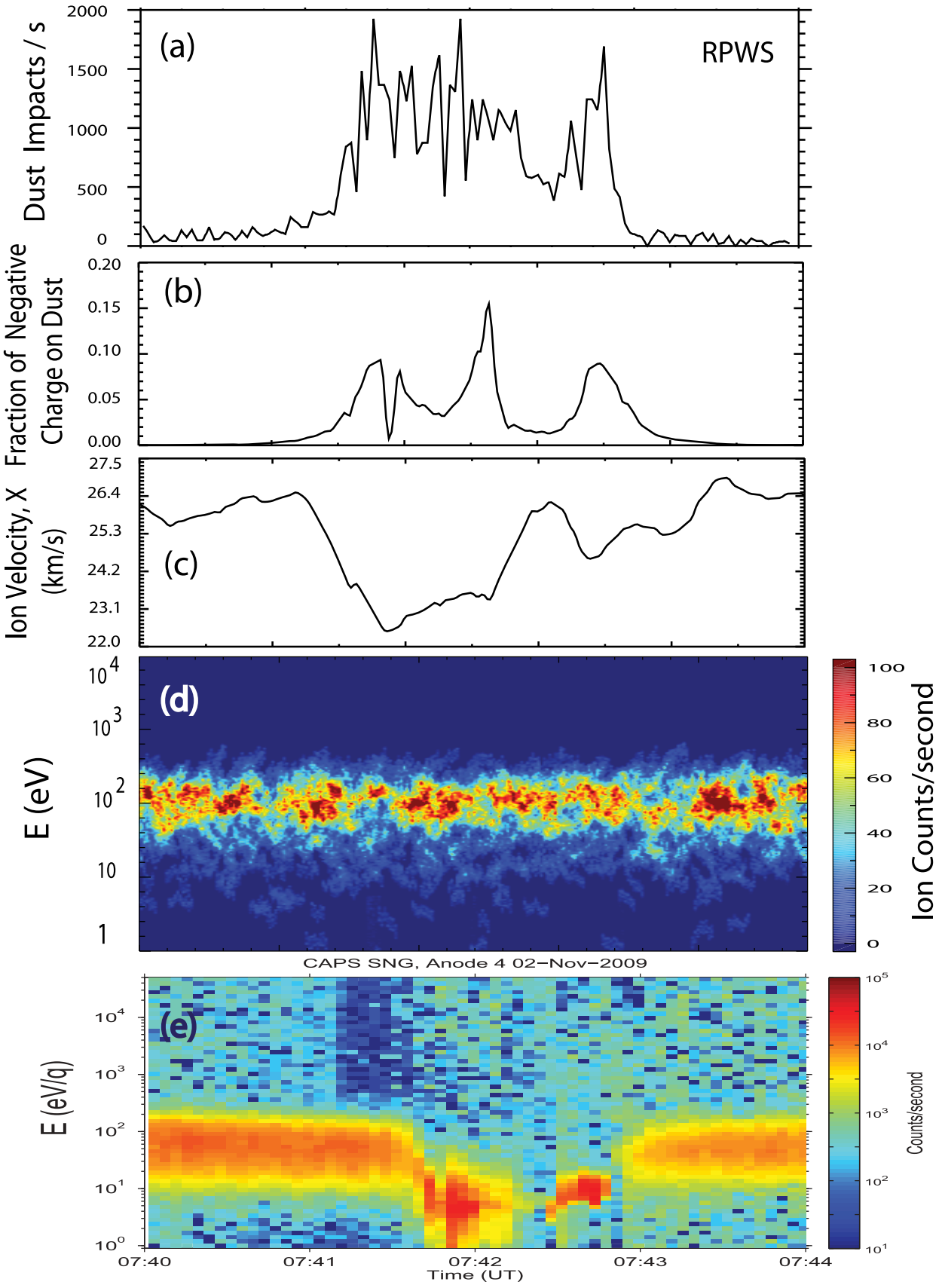


**Figure 9.** (a) RPWS high-sensitivity dust impact rates, (b) fraction of negative charge on dust, (c) X component of flow velocity, (d) simulated ion energy spectrogram, and (e) the CAPS ion energy spectrogram are shown.

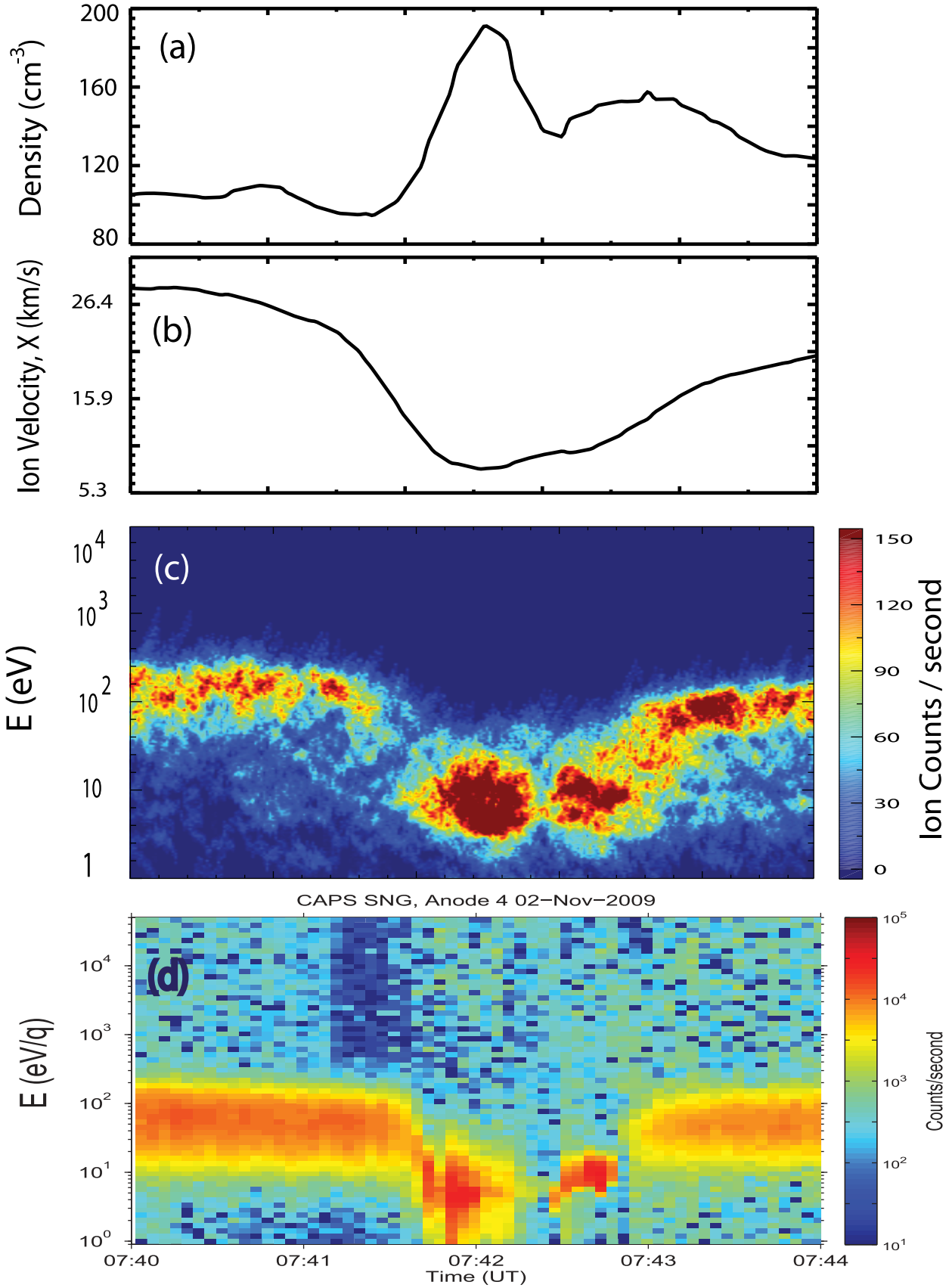


**Figure 10.** (a) Ion density, (b) velocity along X, and (c) ion energy spectrogram from a hybrid run with two neutral gas plumes. The simulation results are in good agreement with the (d) CAPS ion energy spectrogram.

[29] The results presented here indicate that charged dust did not contribute to the observed flow stagnation at Enceladus during E7, even if one allows for the level of electron absorption reported in *Farrell et al.* [2009] during the E3 encounter. Instead, charge exchange between the corotating ions and neutral gas in the plumes plays the dominant role in flow deceleration. This conclusion is in agreement with earlier studies such as *Pontius and Hill* [2006], *Tokar et al.* [2006], *Burger et al.* [2007], and *Fleshman et al.* [2010] who argued for the dominance of charge exchange process in the interaction between the corotating plasma and Enceladus plumes. This dominance is in part due to the fact that the charge exchange cross sections are larger than other processes such as photo ionization [e.g., *Burger et al.*, 2007]. In addition, given that the thermal velocity of the corotating ions is comparable to their flow speed, the process of charge exchange with the neutral gas is extremely efficient in removal of energy and momentum from the plasma.

[30] In general, the extent to which charged dust can impact the flow near Enceladus is dependent on its spatial distribution which varies with the activity level of various plumes at Enceladus with time. Studies similar to this are needed in the future to assess the extent to which charged dust may have contributed to significant flow deceleration during other Cassini flybys of Enceladus. In this study, we have considered dust charging through electron absorption. This process has a limit in that charging of the dust particles cannot continue once local electrons in the plasma have been absorbed. Inclusion of other charging processes, such as triboelectric charging [e.g., *Jones et al.*, 2009] can shine further light on the role of charged dust on flow deceleration.

[31] **Acknowledgments.** We thank the reviewers for their helpful comments and suggestions. Work for this project was supported by NASA contract 1356500 to the University of Iowa with the Jet Propulsion Laboratory.

[32] Philippa Browning thanks the reviewers for their assistance in evaluating this paper.

## References

Burger, M. H., E. C. Sittler Jr., R. E. Johnson, H. T. Smith, O. J. Tucker, and V. I. Shematovich (2007), Understanding the escape of water from Enceladus, *J. Geophys. Res.*, *112*, A06219, doi:10.1029/2006JA012086.

Cowee, M. M., N. Omidi, C. T. Russell, X. Blanco-Cano, and R. L. Tokar (2009), Determining ion production rates near Saturn's extended neutral cloud from ion cyclotron wave amplitudes, *J. Geophys. Res.*, *114*, A04219, doi:10.1029/2008JA013664.

Cravens, T. E., R. L. McNutt Jr., J. H. Waite Jr., I. P. Robertson, J. G. Luhmann, W. Kasprzak, and W.-H. Ip (2009), Plume ionosphere of Enceladus as seen by the Cassini ion and neutral mass spectrometer, *Geophys. Res. Lett.*, *36*, L08106, doi:10.1029/2009GL037811.

Dougherty, M. K., K. K. Khurana, F. M. Neubauer, C. T. Russell, J. Saur, J. S. Leisner, and M. E. Burton (2006), Identification of a dynamic atmosphere of Enceladus with the Cassini magnetometer, *Science*, *311*, 1406–1409, doi:10.1126/science.1120985.

Farrell, W. M., W. S. Kurth, D. A. Gurnett, R. E. Johnson, M. L. Kaiser, J.-E. Wahlund, and J. H. Waite Jr. (2009), Electron density dropout near Enceladus in the context of water-vapor and water-ice, *Geophys. Res. Lett.*, *36*, L10203, doi:10.1029/2008GL037108.

Fleshman, B. L., P. A. Delamere, and F. Bagenal (2010), Modeling the Enceladus plume-plasma interaction, *Geophys. Res. Lett.*, *37*, L03202, doi:10.1029/2009GL041613.

Gurnett, D. A., W. S. Kurth, F. L. Scarf, J. A. Burns, J. N. Cuzzi, and E. Grün (1987), Micron-sized particle impacts detected near Uranus by the Voyager 2 plasma wave instrument, *J. Geophys. Res.*, *92*(A13), 14,959–14,968, doi:10.1029/JA092iA13p14959.

Hansen, C. J., L. Esposito, A. I. F. Stewart, J. Colwell, A. Hendrix, W. Pryor, D. Shemansky, and R. West (2006), Enceladus' water vapor plume, *Science*, *311*, 1422–1425, doi:10.1126/science.1121254.

Hill, T. W., et al. (2012), Charged nanograins in the Enceladus plume, *J. Geophys. Res.*, *117*, A05209, doi:10.1029/2011JA017218.

Jia, Y., C. T. Russell, K. K. Khurana, G. Toth, J. S. Leisner, and T. I. Gombosi (2010a), Interaction of Saturn's magnetosphere and its moons: 1. Interaction between corotating plasma and standard obstacles, *J. Geophys. Res.*, *115*, A04214, doi:10.1029/2009JA014630.

Jia, Y., C. T. Russell, K. K. Khurana, Y. J. Ma, D. Najib, and T. I. Gombosi (2010b), Interaction of Saturn's magnetosphere and its moons: 2. Shape of the Enceladus plume, *J. Geophys. Res.*, *115*, A04215, doi:10.1029/2009JA014873.

Jia, Y.-D., C. T. Russell, K. K. Khurana, Y. J. Ma, W. Kurth, and T. I. Gombosi (2010c), Interaction of Saturn's magnetosphere and its moons: 3. Time variation of the Enceladus plume, *J. Geophys. Res.*, *115*, A12243, doi:10.1029/2010JA015534.

Jones, G. H., E. Roussos, N. Krupp, C. Paranicas, J. Woch, A. Lagg, D. G. Mitchell, S. M. Krimigis, and M. K. Dougherty (2006), Enceladus' varying imprint on the magnetosphere of Saturn, *Science*, *311*, 1412–1415, doi:10.1126/science.1121011.

Jones, G. H., et al. (2009), Fine jet structure of electrically charged grains in Enceladus' plume, *Geophys. Res. Lett.*, *36*, L16204, doi:10.1029/2009GL038284.

Khurana, K. K., M. K. Dougherty, C. T. Russell, and J. S. Leisner (2007), Mass loading of Saturn's magnetosphere near Enceladus, *J. Geophys. Res.*, *112*, A08203, doi:10.1029/2006JA012110.

Kivelson, M. G. (2006), Does Enceladus govern magnetospheric dynamics at Saturn?, *Science*, *311*, 1391–1392, doi:10.1126/science.1124494.

Kriegel, H., S. Simon, J. Müller, U. Motschmann, J. Saur, K.-H. Glassmeier, and M. Dougherty (2009), The plasma interaction of Enceladus: 3D hybrid simulations and comparison with Cassini MAG data, *Planet. Space Sci.*, *57*(14–15), 2113–2122, doi:10.1016/j.pss.2009.09.025.

Kriegel, H., S. Simon, U. Motschmann, J. Saur, F. M. Neubauer, A. M. Persoon, M. K. Dougherty, and D. A. Gurnett (2011), Influence of negatively charged plume grains on the structure of Enceladus' Alfvén wings: Hybrid simulations versus Cassini Magnetometer data, *J. Geophys. Res.*, *116*, A10223, doi:10.1029/2011JA016842.

Kurth, W. S., T. F. Averkamp, D. A. Gurnett, and Z. Wang (2006), Cassini RPWS observations of dust in Saturn's E Ring, *Planet. Space Sci.*, *54*, 988–998, doi:10.1016/j.pss.2006.05.011.

Lee, A. Y., E. K. Wang, E. B. Pilinski, G. A. Macala, and A. Feldman (2010), Estimation and modeling of Enceladus plume jet density using reaction wheel control data, paper presented at AIAA Guidance, Navigation, and Control Conference, Am. Inst. of Aeronaut. and Astronaut., Toronto, Ontario, Canada.

Leisner, J. S., C. T. Russell, M. K. Dougherty, X. Blanco-Cano, R. J. Strangeway, and C. Bertucci (2006), Ion cyclotron waves in Saturn's E ring: Initial Cassini observations, *Geophys. Res. Lett.*, *33*, L11101, doi:10.1029/2005GL024875.

Neubauer, F. M. (1980), Nonlinear standing Alfvén wave current system at Io: Theory, *J. Geophys. Res.*, *85*, 1171–1178, doi:10.1029/JA085iA03p01171.

Omidi, N., C. T. Russell, R. L. Tokar, and J. S. Leisner (2010a), Hybrid simulations of the plasma environment around Enceladus, *J. Geophys. Res.*, *115*, A05212, doi:10.1029/2009JA014391.

Omidi, N., C. T. Russell, R. L. Tokar, W. M. Farrell, W. S. Kurth, D. A. Gurnett, Y. D. Jia, and J. S. Leisner (2010b), Hybrid simulations of plasma-neutral-dust interactions at Enceladus, in *Pickup Ions Throughout the Heliosphere and Beyond*, edited by J. A. le Roux et al., *AIP Conf. Proc.*, *1303*, 237–242.

Pontius, D. H., Jr., and T. W. Hill (2006), Enceladus: A significant plasma source for Saturn's magnetosphere, *J. Geophys. Res.*, *111*, A09214, doi:10.1029/2006JA011674.

Porco, C. C., et al. (2006), Cassini observes the active south pole of Enceladus, *Science*, *311*, 1393–1401, doi:10.1126/science.1123013.

Saur, J., F. M. Neubauer, and N. Schilling (2007), Hemisphere coupling in Enceladus' asymmetric plasma interaction, *J. Geophys. Res.*, *112*, A11209, doi:10.1029/2007JA012479.

Saur, J., N. Schilling, F. M. Neubauer, D. F. Strobel, S. Simon, M. K. Dougherty, C. T. Russell, and R. T. Pappalardo (2008), Evidence for temporal variability of Enceladus' gas jets: Modeling of Cassini observations, *Geophys. Res. Lett.*, *35*, L20105, doi:10.1029/2008GL035811.

Shafiq, M., J.-E. Wahlund, M. W. Morooka, W. S. Kurth, and W. M. Farrell (2011), Characteristics of the dust-plasma interaction near Enceladus' South Pole, *Planet. Space Sci.*, *59*, 17–25, doi:10.1016/j.pss.2010.10.006.

Simon, S., J. Saur, H. Kriegel, F. M. Neubauer, U. Motschmann, and M. K. Dougherty (2011), Influence of negatively charged plume grains and hemisphere coupling currents on the structure of Enceladus' Alfvén wings: Analytical modeling of Cassini magnetometer observations, *J. Geophys. Res.*, *116*, A04221, doi:10.1029/2010JA016338.

Smith, H. T., R. E. Johnson, M. E. Perry, D. G. Mitchell, R. L. McNutt, and D. T. Young (2010), Enceladus plume variability and the neutral gas

densities in Saturn's magnetosphere, *J. Geophys. Res.*, *115*, A10252, doi:10.1029/2009JA015184.

Spencer, J. R., J. C. Pearl, M. Segura, F. M. Flasar, A. Mamoutkine, P. Romani, B. J. Buratti, A. R. Hendrix, L. J. Spilker, and R. M. C. Lopes (2006), Cassini encounters Enceladus: Background and discovery of a south polar hot spot, *Science*, *311*, 1401–1405, doi:10.1126/science.1121661.

Tokar, R. L., et al. (2006), The interaction of the atmosphere of Enceladus with Saturn's plasma, *Science*, *311*, 1409–1412, doi:10.1126/science.1121061.

Tokar, R. L., R. E. Johnson, M. F. Thomsen, R. J. Wilson, D. T. Young, F. J. Crary, A. J. Coates, G. H. Jones, and C. S. Paty (2009), Cassini detection of Enceladus' cold water-group plume ionosphere, *Geophys. Res. Lett.*, *36*, L13203, doi:10.1029/2009GL038923.

Waite, H. J., Jr., et al. (2006), Cassini ion and neutral mass spectrometer: Enceladus plume composition and structure, *Science*, *311*, 1419–1422, doi:10.1126/science.1121290.

Wang, Z., D. A. Gurnett, T. F. Averkamp, A. M. Persoon, and W. S. Kurth (2006), Characteristics of dust particles detected near Saturn's ring plane with the Cassini Radio and Plasma Wave Instrument, *Planet. Space Sci.*, *54*, 957–966, doi:10.1016/j.pss.2006.05.015.